Letters

A Fast Positive Sequence Components Extraction Method With Noise Immunity in Unbalanced Grids

Liwei Du, Mingxian Li, Zhen Tang, Liansong Xiong, *Member, IEEE*, Xun Ma, and Guoxin Tang

***Abstract*—Fast and accurate acquisition of voltage components is the basic requirement for grid-tied inverters to realize various control under unbalanced grids. In view of this situation, a delay sampling period filter, which rapidly separates each voltage component by delaying two sampling periods in *dq* frame, is proposed in this article. In view of the noise interference, a delay operation period filter (DOPF) is proposed to scale the operation period and limit the noise to an acceptable range. The complete positive sequence components (PSC) extraction method based on the developed DOPF+ moving average filter (MAF) algorithm is presented, combing the advantages of DOPF and MAF for eliminating the double-frequency ac components and high-frequency noise, respectively. Finally, the feasibility and priority of the DOPF+MAF algorithm and PSC extraction method have been verified by the physical experimental results.**

***Index Terms*—Delay operation period filter (DOPF) algorithm, noise immunity, positive sequence components (PSCs), unbalanced grid.**

I. Introduction

THE FAST and accurate acquisition of positive sequence components (PSC) of unbalanced grid voltage is an essential condition to ensure the normal operation of the grid-connected inverter and realize various control [1], [2].

When the grid voltage is unbalanced, the dc components and double-frequency ac components appear in *dq* frame. Filters are usually designed to filter out the double-frequency ac components, and the pure dc components can be extracted. Most existing ac components elimination methods are based on the various low-pass filters, which are difficult to make an ideal compromise between the dynamic response speed and the ac attenuation ability [3]. In [4] and [5], the delay signal cancellation (DSC) method is used to separate PSC and negative sequence components (NSC), but it delays 1/4 grid period. In [6]–[8], cascaded DSC block with different time delays can eliminate several harmonics. In [9]–[11], a comparison between DSC and moving average filter (MAF) is made, showing that these two methods are mathematically equivalent under certain conditions and that MAF also has the problem of slow response. The method in [12] adopts only one DSC module and one MAF module to eliminate NSCs. However, the MAF introduces a time delay that equals to the window length of MAF. In [13], the generalized DSC algorithm is used as the prefilter of phase locked loop (PLL), and it could extract the PSCs by delaying a line frequency period. In [14], adaptive notch filter (ANF) is incorporated into the PLL to eliminate the harmonic components of the required frequency selectively. Still, the ANF cannot treat the NSCs. In [15], a dual second-order generalized integrator (DSOGI) is used to extract the PSCs of grid voltage. However, the DSOGI filter can hardly filter out the low frequency components. The decoupled double synchronous reference frame in [16] can detect both PSC and NSC at the cost of heavy complexity and computational burden. Besides, some innovative technologies for grid frequency estimation are worthy being introduced into the PSCs extraction, including the three consecutive samples technology in [17] and the complex-valued least-squares framework in [18]. But unlike the application scenario of the power system frequency estimation, for the embedded controller based grid-tied converter system, the corresponding algorithms shall be simple, reliable and easy to implement, and can be completed within the switching period of power electronics (generally at ms level).

Therefore, to further improve the response speed of the PSC extraction, this letter proposes a delay operation period filter (DOPF) algorithm in *dq* frame characterized by the fastest response, easy implementation and strong noise immunity. Comparing with the classical DSC, MAF, and DSOGI schemes, the obvious advantages of the developed DOPF+MAF algorithm and PSC extraction method in response speed have been verified through physical experiments.

Manuscript received October 14, 2019; revised November 19, 2019 and December 7, 2019; accepted December 9, 2019. Date of publication December 11, 2019; date of current version March 13, 2020. The work was supported in part by the National Natural Science Foundation of China under Grant 51707091. *(Corresponding author: Liansong Xiong.)*

L. Du and X. Ma are with Solar Energy Research Institute, Yunnan Normal University, Kunming 650500, China (e-mail: 1205977155@qq.com; 46946599@qq.com).

M. Li is with the College of Electrical and Power Engineering, China University of Mining and Technology, Xuzhou 221116, China (e-mail: 1425385799@qq.com).

Z. Tang is with State Grid Shanxi Electric Power Corporation Electric Power Research Institute, Taiyuan 0300001, China (e-mail: tangzhen @sx.sgcc.com.cn).

L. Xiong is with the School of Automation, Nanjing Institute of Technology, Nanjing 210036, China, and also with the School of Electrical Engineering, Xi'an Jiaotong University, Nanjing 710049, China (e-mail: xiongliansong@163.com).

G. Tang is with the College of Information and Business, North University of China, Jinzhong 030600, China (e-mail: 1320372112@qq.com).

Color versions of one or more of the figures in this article are available online at http://ieeexplore.ieee.org.

Digital Object Identifier 10.1109/TPEL.2019.2959672

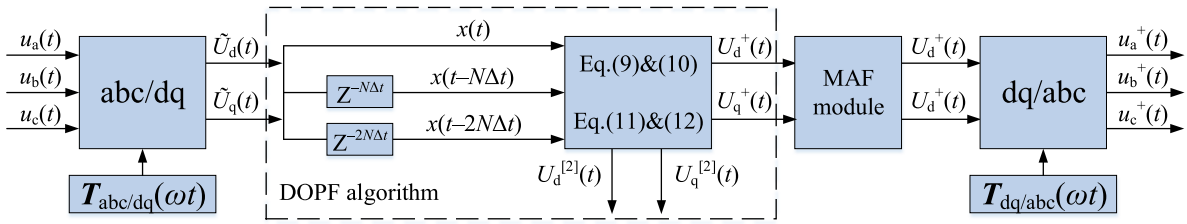

Fig. 1. PSCs extraction method of unbalanced grid voltage.

II. DSPF Algorithm

According to the symmetrical component method, the asymmetric grid voltage can be expressed as

$$\mathbf{U} = \boldsymbol{U}^+ + \boldsymbol{U}^- \tag{1}$$

where, $\boldsymbol{U}^+$ and $\boldsymbol{U}^-$ are PSC and NSC voltages, respectively.

To simplify the analysis process, only the NSC is taken as an example in this paper to illustrate the impact on the sequence components extraction in *dq* frame.

According to (1), PSC and NSC voltages can be rewritten as

$$\boldsymbol{U}^+ = \begin{bmatrix} u_{\mathrm{a}}^+(t) \\ u_{\mathrm{b}}^+(t) \\ u_{\mathrm{c}}^+(t) \end{bmatrix} = \begin{bmatrix} U_{\mathrm{m}}^+ \sin(\omega t + \theta) \\ U_{\mathrm{m}}^+ \sin(\omega t - 2\pi/3 + \theta) \\ U_{\mathrm{m}}^+ \sin(\omega t + 2\pi/3 + \theta) \end{bmatrix} \tag{2}$$

$$\boldsymbol{U}^- = \begin{bmatrix} u_{\mathrm{a}}^-(t) \\ u_{\mathrm{b}}^-(t) \\ u_{\mathrm{c}}^-(t) \end{bmatrix} = \begin{bmatrix} U_{\mathrm{m}}^- \sin(\omega t + \delta) \\ U_{\mathrm{m}}^- \sin(\omega t + 2\pi/3 + \delta) \\ U_{\mathrm{m}}^- \sin(\omega t - 2\pi/3 + \delta) \end{bmatrix} \tag{3}$$

where ω is the grid frequency; u_{abc}^i is the sequence components of unbalanced voltages and *i* is either + or –; $\boldsymbol{U}_{\mathrm{m}}^+$ and $\boldsymbol{U}_{\mathrm{m}}^-$ are amplitudes of PSC and NSC, respectively; and θ and δ are the initial phases of PSC and NSC, respectively.

After abc/dq Transformation [11], (1) can be rewritten as

$$\begin{cases} U_{\mathrm{d}} = U_{\mathrm{m}}^+ \cos\theta - U_{\mathrm{m}}^- \cos(2\omega t + \delta) \\ U_{\mathrm{q}} = U_{\mathrm{m}}^+ \sin\theta + U_{\mathrm{m}}^- \sin(2\omega t + \delta). \end{cases} \tag{4}$$

Therefore, when the grid voltage is unbalanced, the dc components and double-frequency ac components appear in dq frame. At present, the fastest DSC filter requires at least 1/4 grid period to eliminate the ac component [4], [5]. Therefore, this articles proposes a DSPF to eliminate the double-frequency ac components, which can further reduce the response time.

The voltage components extraction scheme based on the proposed DSPF algorithm is as follows. DC components and double-frequency ac components are extracted by delaying two sampling periods of voltage component in *dq* frame. The operating principle is shown in Fig. 1.

Replace *t* in (4) with $t + \Delta t$ and $t - \Delta t$, respectively, we can get (5), (6), and (7), (8), shown at the bottom of this page.

Solving simultaneous (5), (6), and (7), (8) as well, then the dc components of U_{d} and U_{q} can be obtained, respectively, which can be calculated by

$$\begin{aligned} U_{\mathrm{d}}^+ &= U_{\mathrm{m}}^+ \cos\theta \\ &= \frac{U_{\mathrm{d}}(t+\Delta t) + U_{\mathrm{d}}(t-\Delta t) - 2U_{\mathrm{d}}(t)\cos(2\omega\Delta t)}{2\left[1-\cos(2\omega\Delta t)\right]} \end{aligned} \tag{9}$$

$$\begin{aligned} U_{\mathrm{q}}^+ &= U_{\mathrm{m}}^+ \sin\theta \\ &= \frac{U_{\mathrm{q}}(t+\Delta t) + U_{\mathrm{q}}(t-\Delta t) - 2U_{\mathrm{q}}(t)\cos(2\omega\Delta t)}{2\left[1-\cos(2\omega\Delta t)\right]}. \end{aligned} \tag{10}$$

Similarly, the double-frequency AC components can be obtained by

$$\begin{aligned} U_{\mathrm{d}}^{[2]} &= U_{\mathrm{m}}^- \cos(2\omega t + \delta) \\ &= \frac{U_{\mathrm{d}}(t+\Delta t) + U_{\mathrm{d}}(t-\Delta t) - 2U_{\mathrm{d}}(t)}{2\left[1-\cos(2\omega\Delta t)\right]} \end{aligned} \tag{11}$$

$$\begin{aligned} U_{\mathrm{q}}^{[2]} &= U_{\mathrm{m}}^- \sin(2\omega t + \delta) \\ &= \frac{U_{\mathrm{q}}(t+\Delta t) + U_{\mathrm{q}}(t-\Delta t) - 2U_{\mathrm{q}}(t)}{2\left[\cos(2\omega\Delta t)-1\right]}. \end{aligned} \tag{12}$$

The proposed trigonometric transformation-based algorithm is a typical open-loop detection system that does not contain the closed-loop feedback unit and the controlled objects carrying disturbances. Its output is bounded for every bounded input. Therefore, according to bounded input bounded output (BIBO) criterion [19], the DOPF algorithm is BIBO stable and its stability is promised.

III. Noise Immunity Analysis

Taking the filtering of double-frequency AC components in $U_{\mathrm{d}}(t)$ as an example (similarly for $U_{\mathrm{q}}(t)$), the dc components in the *k*th sampling can be described as follows:

$$x_{\mathrm{d}}^+(k) = \frac{x(k) + x(k-2) - 2x(k-1)\cos(2\omega\Delta t)}{2\left[1-\cos(2\omega\Delta t)\right]}. \tag{13}$$

$$U_{\mathrm{d}}(t+\Delta t) = U_{\mathrm{d}}\cos(2\omega\Delta t) + U_{\mathrm{q}}\sin(2\omega\Delta t) + U_{\mathrm{m}}^+\cos\theta\left[1-\cos(2\omega\Delta t)\right] - U_{\mathrm{m}}^+\sin\theta\sin(2\omega\Delta t) \tag{5}$$

$$U_{\mathrm{d}}(t-\Delta t) = U_{\mathrm{d}}\cos(2\omega\Delta t) - U_{\mathrm{q}}\sin(2\omega\Delta t) + U_{\mathrm{m}}^+\cos\theta\left[1-\cos(2\omega\Delta t)\right] + U_{\mathrm{m}}^+\sin\theta\sin(2\omega\Delta t) \tag{6}$$

$$U_{\mathrm{q}}(t+\Delta t) = U_{\mathrm{q}}\cos(2\omega\Delta t) - U_{\mathrm{d}}\sin(2\omega\Delta t) + U_{\mathrm{m}}^+\sin\theta\left[1-\cos(2\omega\Delta t)\right] + U_{\mathrm{m}}^+\cos\theta\sin(2\omega\Delta t) \tag{7}$$

$$U_{\mathrm{q}}(t-\Delta t) = U_{\mathrm{q}}\cos(2\omega\Delta t) + U_{\mathrm{d}}\sin(2\omega\Delta t) + U_{\mathrm{m}}^+\sin\theta\left[1-\cos(2\omega\Delta t)\right] - U_{\mathrm{m}}^+\cos\theta\sin(2\omega\Delta t) \tag{8}$$

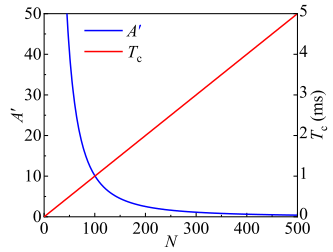

Fig. 2. Noise amplification factor and sampling period versus scaling factor.

When considering the high-frequency random noise, (13) can be redescribed as

$$\begin{aligned}\tilde{x}_{\mathrm{d}}^{+}(k) &= \frac{\tilde{x}(k)+\tilde{x}(k-2)-2\tilde{x}(k-1)\cos(2\omega\Delta t)}{2[1-\cos(2\omega\Delta t)]}\\ &= \frac{[x_{\mathrm{d}}(k)+x_{\mathrm{n}}(k)]+[x_{\mathrm{d}}(k-2)+x_{\mathrm{n}}(k-2)]}{2[1-\cos(2\omega\Delta t)]}\\ &\quad-\frac{[x_{\mathrm{d}}(k-1)+x_{\mathrm{n}}(k-1)]\cos(2\omega\Delta t)}{1-\cos(2\omega\Delta t)}\\ &= x_{\mathrm{d}}^{+}(k)+x_{\mathrm{n\_d}}(k)\end{aligned} \tag{14}$$

and

$$\begin{aligned}x_{\mathrm{n\_d}}(k) &= \frac{x_{\mathrm{n}}(k)+x_{\mathrm{n}}(k-2)-2x_{\mathrm{n}}(k-1)\cos(2\omega\Delta t)}{2[1-\cos(2\omega\Delta t)]}\\ &\le \frac{|x_{\mathrm{n}}(k)|+|x_{\mathrm{n}}(k-2)|+2|x_{\mathrm{n}}(k-1)|\cos(2\omega\Delta t)}{2[1-\cos(2\omega\Delta t)]}\\ &\le |x_{\mathrm{n}}|\frac{1+\cos(2\omega\Delta t)}{1-\cos(2\omega\Delta t)}\\ &= |x_{\mathrm{n}}|\frac{\cos^2(\omega\Delta t)}{\sin^2(\omega\Delta t)} = |x_{\mathrm{n}}|A_{\max}\end{aligned} \tag{15}$$

where $|x_{\mathrm{n}}|$ is the maximum noise value possible; and $A_{\max}$ is the noise amplification factor under the worst conditions. And

$$A_{\max} = \frac{\cos^2(\omega\Delta t)}{\sin^2(\omega\Delta t)}. \tag{16}$$

Apparently

$$\lim_{\Delta t\to 0} A_{\max} = \lim_{\Delta t\to 0}\frac{\cos^2(\omega\Delta t)}{\sin^2(\omega\Delta t)} = \frac{1}{(\omega\Delta t)^2} = \left(\frac{f_{\mathrm{s}}}{\omega}\right)^2. \tag{17}$$

The accuracy of the proposed filtering method cannot be reduced with the decrease of sampling frequency. Therefore, the operation period in DSPF algorithm can be scaled to limit the noise to an acceptable range, i.e., DOPF.

Let's define the operation period T_{c} as

$$T_{\mathrm{c}} = N\Delta t. \tag{18}$$

In (18), N is the scaling factor of the sampling time interval. Obviously, the response time of DOPF is the same as the operation period. Replace the sampling period in DSPF by the operation period in (18). At this point, the maximum noise amplification factor of DOPF is

$$A' = \frac{\cos^2(\omega N\Delta t)}{\sin^2(\omega N\Delta t)}. \tag{19}$$

Meanwhile, it can be seen from Fig. 2 that the response time under the worst conditions increases linearly with the increase of N ($f_{\mathrm{s}} = 100$ kHz). The maximum noise amplification factor decreases significantly with the increase of N. N can be compromised according to the random noise in practical application scenarios, which can effectively reduce noise and ensure the relatively fast response speed.

The theoretical range of N in the actual application scenarios can be calculated according to detected signal-noise ratio (SNR) indicator and the allowable SNR of the power electronic system. According to Fig. 2, N can be specifically selected according to the industrial application conditions.

Besides, after quickly eliminating the double-frequency ac components in dq frame, an MAF block in series is employed to completely filter out the remaining high-frequency random noise [9]–[13], combing the advantages of DOPF and MAF for eliminating the double-frequency ac components and high-frequency noise, respectively. Therefore, the complete PSC extraction method based on the presented DOPF+MAF algorithm shown in Fig. 1 is characterized by fast response speed, easy implantation and strong noise immunity.

IV. Experimental Verification

To verify the developed algorithm, TMS320F28335 DSP is used as the core controller to realize the algorithm verification. The unbalanced grid voltage signal is simulated by real-time simulation platform, and the sampling frequency is 20 kHz. The algorithm outputs, including PSCs and real-time phase, are transferred to an oscilloscope through a D/A converter additionally provided by the digital control system. In the experimental scenario, the unbalanced grid voltage working condition occurs suddenly, as shown in Fig. 3(a).

Besides, the operation cycle of the DOPF algorithm is 30 times the sampling period to ensure that the noise is within the acceptable range, and the MAF with a cut-off frequency of 670 Hz are connected in series to reduce the high-frequency noise in dq frame. In addition, a saturation module is inserted between DOPF and MAF blocks to reduce the overshooting during the dynamic process.

First, the DOPF+MAF algorithm is compared with DSC, MAF, and DSOGI algorithms, as shown in Fig. 3(b) and (c). Experimental results show that the double-frequency ac components on the d-axis and q-axis can be effectively eliminated by the four algorithms. However, as shown in Fig. 4, the response times of DOPF+MAF, DSC, MAF, and DSOGI algorithms are quite different: 3 ms, 5 ms, 10 ms, and more than 20 ms, respectively. Obviously, the developed algorithm possesses the shortest response time, which is 40% and 70% shorter than that of the DSC and MAF algorithm. Besides, the developed algorithm is also free from the noise issues, which is critical for engineering applications.

Two typical applications, PSC and phase detections, were verified, as shown in Fig. 3(d) and (e), respectively. The PSCs of unbalanced grid voltage are detected by the algorithm in Fig. 1 and the grid phase detection is realized by the fast open-loop phase locking scheme in [20], whose double-frequency

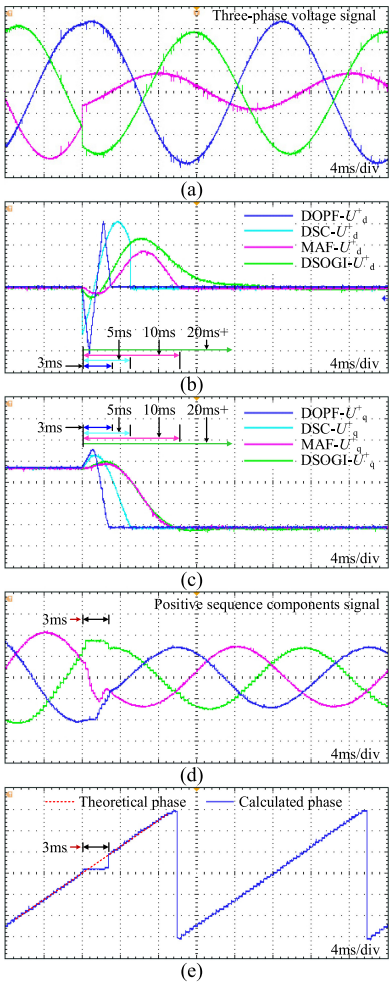

Fig. 3. Experimental results.

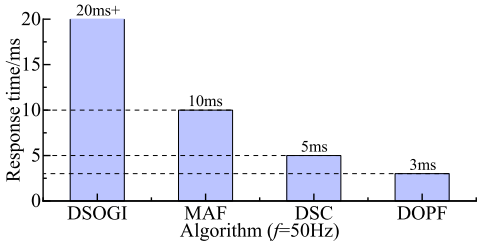

Fig. 4. Response time of different filter algorithms.

ac components are filtered all by the developed DOPF+MAF algorithm. The experimental results show that both applications are well carried out and achieve the fastest response speed with the help of the developed algorithm.

V. Conclusion

The proposed DOPF algorithm can completely filter out the double-frequency ac components in *dq* frame quickly and accurately. The response time of the developed algorithm is 40% and 70% shorter than that of the classical DSC and MAF algorithm, which is vital for high-performance control of grid-tied converters. Besides, it is also free from the noise issues, which is of critical importance for the engineering applications. The developed algorithm is also applicable to phase detection, sequence components separation, power quality control, grid fault ride through for power converter control, etc.

References

[1] X. Guo, W. Liu, and Z. Lu, "Flexible power regulation and current-limited control of the grid-connected inverter under unbalanced grid voltage faults," *IEEE Trans. Power Electron.*, vol. 64, no. 9, pp. 7425–7432, Feb. 2017.

[2] L. Xiong *et al.*, "Static synchronous generator model: a new perspective to investigate dynamic characteristics and stability issues of grid-tied PWM inverter," *IEEE Trans. Power Electron.*, vol. 31, no. 9, pp. 6264–6280, Sep. 2016.

[3] P. Kanjiya, V. Khadkikar, and M. S. El Moursi, "Adaptive low-pass filter based DC offset removal technique for three-phase PLLs," *IEEE Trans. Ind. Electron.*, vol. 65, no. 11, pp. 9025–9029, Mar. 2018.

[4] M. Rasheduzzaman and J. W. Kimball, "Modeling and tuning of an improved delayed-signal-cancellation PLL for microgrid application," *IEEE Trans. Energy Convers.*, vol. 34, no. 2, pp. 712–721, Nov. 2019.

[5] S. Golestan *et al.*, "Advanced single-phase DSC-based PLLs," *IEEE Trans. Power Electron.*, vol. 34, no. 4, pp. 3226–3238, Jul. 2018.

[6] S. Golestan, M. Ramezani, J. M. Guerrero, and M. Monfared, "dq-frame cascaded delayed signal cancellation- based PLL: Analysis, design, and comparison with moving average filter-based PLL," *IEEE Trans. Power Electron.*, vol. 30, no. 3, pp. 1618–1632, Mar. 2015.

[7] Y. F. Wang and Y. W. Li, "Three-phase cascaded delayed signal cancellation PLL for fast selective harmonic detection," *IEEE Trans. Ind. Electron.*, vol. 60, no. 4, pp. 1452–1463, Apr. 2013.

[8] S. Gude and C. Chu, "Three-phase PLLs by using frequency adaptive multiple DSC prefilters under adverse grid conditions," *IEEE Trans. Ind. Appl.*, vol. 54, no. 4, pp. 3832–3844, Jul. 2018.

[9] L. Xiong, X. Liu, C. Zhao, and F. Zhuo, "A fast and robust real-time detection algorithm of decaying dc transient and harmonic components in three-phase systems," *IEEE Trans. Power Electron.*, 2019, to be published.

[10] S. Golestan, J. M. Guerrero, A. Vidal, A. G. Yepes, and J. Doval-Gandoy, "PLL with MAF-based prefiltering stage: Small-signal modeling and performance enhancement," *IEEE Trans. Power Electron.*, vol. 31, no. 6, pp. 4013–4019, Jun. 2016.

[11] L. Xiong *et al.*, "A quantitative evaluation and comparison of harmonic elimination algorithms based on MAF and DSC in phase synchronization applications," *J. Power Electron.*, vol. 16, no. 2, pp. 717–730, Mar. 2016.

[12] S. Golestan, J. M. Guerrero, A. M. Abusorrah, and Y. Al-Turki, "Hybrid synchronous/stationary reference-frame-filtering-based PLL," *IEEE Trans. Ind. Electron.*, vol. 62, no. 8, pp. 5018–5022, Jan. 2015.

[13] S. D. S. Andrade, Y. N. Batista, F. A. S. Neves, and H. E. P. De Souza, "Fast phase angle jump estimation to improve the convergence time of the GDSC-PLL," *IEEE Trans. Power Electron.*, vol. 67, no. 4, pp. 2852–2862, Apr. 2020.

[14] X. He, H. Geng, and G. Yang, "A generalized design framework of notch filter based frequency-locked loop for three-phase grid voltage," *IEEE Trans. Ind. Electron.*, vol. 65, no. 9, pp. 7072–7084, Dec. 2018.

[15] C. Zhang, X. Zhao, X. Wang, X. Chai, Z. Zhang, and X. Guo, "A grid synchronization PLL method based on mixed second- and third-order generalized integrator for DC offset elimination and frequency adaptability," *IEEE J. Emerg. Sel. Topics Power Electron.*, vol. 6, no. 3, pp. 1517–1526, Feb. 2018.

[16] Y. Wang, X. Chen, Y. Wang, and C. Gong, "Analysis of frequency characteristics of phase-locked loops and effects on stability of three-phase grid-connected inverter," *Int. J. Electr. Power Energy Syst.*, vol. 113, pp. 652–663, Dec. 2019.

[17] M. S. Reza, M. Ciobotaru, and V. G. Agelidis, "A robust frequency estimation technique based on three consecutive samples for single-phase systems," *IEEE J. Emerg. Sel. Topics Power Electron.*, vol. 2, no. 4, pp. 1049–1058, Dec. 2014.

[18] Y. Xia, Y. He, K. Wang, W. Pei, Z. Blazic, and D. P. Mandic, "A complex least squares enhanced smart dft technique for power system frequency estimation," *IEEE Trans. Power Del.*, vol. 32, no. 3, pp. 1270–1278, Jun. 2017.

[19] P. Li, S. Zhong, and W. Zhao, "Improvement on BIBO stabilization for switched system with time-varying delays," in *Proc. 32nd Youth Acad. Annu. Conf. Chin. Assoc. Automat.*, 2017, pp. 628–633.

[20] L. Xiong *et al.*, "A novel fast open-loop phase locking scheme based on synchronous reference frame for three-phase non-ideal power grids," *J. Power Electron.*, vol. 16, no. 4, pp. 1513–1525, Jul. 2016.